Bioorg. Med. Chem. 121 (2025) 118124

Contents lists available at ScienceDirect

Bioorganic & Medicinal Chemistry

journal homepage: www.elsevier.com/locate/bmc

Design, synthesis and *in vitro* validation of bivalent binders of SARS-CoV-2 spike protein: Obeticholic, betulinic and glycyrrhetinic acids as building blocks☆

Martina Pedrini [a,1], Luca Pozzi [a,1], Francesca Sacchi [a], Andrea Citarella [a,*], Valerio Fasano [a], Pierfausto Seneci [a], Stefano Pieraccini [a], Lorenzo Ruberto [a], Helena Perez Peña [a], Alfredo Garzino-Demo [b,d,e], Adriana Vitiello [b], Leonardo Sernicola [c], Alessandra Borsetti [c], Arianna Calistri [b], Cristina Parolin [b], Daniele Passarella [a,*]

[a] *Department of Chemistry, University of Milan, Via Golgi 19, 20133 Milano, Italy*
[b] *Department of Molecular Medicine, University of Padova, Via Gabelli 63, 35121 Padova, Italy*
[c] *National HIV/AIDS Research Center (CNAIDS), Istituto Superiore di Sanità, 00162 Roma, Italy*
[d] *Department of Microbial Pathogenesis, University of Maryland School of Dentistry, Baltimore, MD 21201, United States*
[e] *Department of Microbiology and Immunology, University of Maryland School of Medicine, Baltimore, MD 21201, United States*

A R T I C L E I N F O

Keywords:
Synthesis
SARS-CoV-2
SPIKE protein
Coronavirus
Natural products
Bivalent binders
Medicinal chemistry
Organic chemistry

A B S T R A C T

SARS-CoV-2 is the virus responsible for the COVID-19 pandemic, which caused over 6.7 million deaths worldwide. The Spike protein plays a crucial role in the infection process, mediating the binding of the virus to its cellular receptor, angiotensin-converting enzyme 2 (ACE2), and its subsequent entry into target cells. Previous studies identified, through virtual screening, several natural products capable of binding to two distinct pockets of the Spike protein: triterpenoids binding to pocket 1 and bile acid derivatives binding to pocket 5. Building on these findings, our study advances the field by developing bivalent compounds **1–4** that through a spacer combine a triterpenoid (betulinic acid or glycyrrhetinic acid) with a semisynthetic bile acid derivative (obeticholic acid). These bivalent compounds are designed to simultaneously bind both pockets of the Spike protein, offering significant advantages over single molecules or the combination of the two natural products. *In vitro* cell assays using pseudotyped recombinant lentiviral particles with selected SARS-CoV-2 Spike proteins demonstrated that **1** and **2** exhibit enhanced activity in reducing viral entry into target cells compared to individual natural products, thus highlighting their potential as superior antiviral agents with reduced side effects.

1. Introduction

Coronaviruses are positive-stranded RNA viruses that belong to the *Coronaviridae* family[1] causing a remarkable variety of human respiratory tract infections from common cold to more serious respiratory diseases.[2,3] SARS-CoV-2 was first identified in Wuhan, China, in December 2019, and nowadays is responsible for the respiratory tract infection COVID-19[4] that caused more than 6.7 million deaths worldwide.[5] The ongoing development of new antiviral therapies for SARS-CoV-2 is essential for effectively treating the infection, especially in anticipation of emerging viral variants that may show resistance to existing treatments and vaccines. Current antiviral drugs for SARS-CoV-2 act through two main mechanisms: 1) preventing the binding between the virus and its host cell receptor, and 2) interfering with viral replication. SARS-CoV-2 attacks host cells through its envelope Spike (S) glycoprotein, located on the viral surface.[6–8] The S protein is a homotrimer composed of two subunits, S1 and S2. In each S1 subunit a receptor binding domain (RBD)[9,10] drives the direct virus binding to the angiotensin-converting enzyme 2 (ACE2) receptor present on target cells.[11,12] This S/ACE2 interaction represents the early stage of virus entry into the host cell, making the S protein an attractive target for antiviral therapeutics. In 2020, Carino et al. conducted an exploratory

☆ This article is part of a special issue entitled: 'Bryan Dickinson' published in Bioorganic & Medicinal Chemistry.

* Corresponding authors.
E-mail addresses: andrea.citarella@unimi.it (A. Citarella), daniele.passarella@unimi.it (D. Passarella).

[1] contributed equally authors.

https://doi.org/10.1016/j.bmc.2025.118124
Received 16 January 2025; Received in revised form 12 February 2025; Accepted 17 February 2025
Available online 18 February 2025

campaign using natural substances and clinically available FDA-approved drugs (2906 drugs from DrugBank and Selleckchem websites) to identify anti-SARS-CoV-2 compounds targeting the viral S protein to block recognition and internalization processes.[13] The combination of an *in silico* approach, based on virtual screening of the β-sheet core of the receptor-binding domain (RBD), and *in vitro* testing, using a screening kit for S/ACE2 inhibitors, resulted in the identification of two classes of natural products that interfere with the RBD/ACE2 binding.[13] Virtual screening identified six binding pockets on the trimeric structure of the S protein (Fig. 1). The results indicate that triterpenoids and steroid compounds exhibit strong selective binding to pocket 1 within the RBD, whereas primary and secondary bile acids, along with their amidated and semi-synthetic derivatives, show higher affinity scores for pocket 5. Importantly, these natural scaffolds were able to inhibit the RBD/ACE2 interaction, confirming that targeting pockets 1 and 5 could be an efficacious strategy to develop anticoronavirus compounds.

Pursuing our interest in developing anticoronavirus compounds[14–17] and the use of natural products as building blocks,[18,19] in this work we designed and synthesized bivalent compounds **1–4** (Fig. 2) to target pockets 1 and 5 of the S protein. This strategy aimed to bind to both pockets simultaneously, rather than using a combination of two distinct drugs, achieving an enhanced biological effect compared with that of the individual natural products and reducing their side effects. Betulinic acid methyl ester (BAME, **5**) and glycyrrhetinic acid methyl ester (GAME, **12**) were selected as ligands of the S protein pocket 1, while obeticholic acid (OCA) was chosen as ligand of pocket 5 (Fig. 2). The moieties were linked either through an aliphatic carbon chain or a longer triazole–based spacer. Bivalent compounds **1–4** were tested for their capability to reduce viral internalization. Two S proteins were assessed, namely a Spike protein bearing the D614G mutation and the Spike protein of the Omicron variant (sublineage BA.2). The D614G mutation appeared early during SARS-CoV-2 spreading in the human population, and was responsible for an increased entry efficiency as well as for an enhanced ACE2-binding affinity.[20] On the other hand, the Omicron variant was firstly reported in November 2021[21] and is still circulating with several sublineages. The Omicron S proteins display several aminoacid changes with respect to the S protein of the original Wuhan virus.[22] Thus, the tested S proteins are representative of both early and late variants of SARS-CoV-2. Among the developed compounds, **1** and **2** consistently showed a significant effect on viral internalization in ACE2 overexpressing eukaryotic cells, achieving a notable reduction for both the D614G and the Omicron variants. These compounds represent potential versatile candidates for combating viral infections.

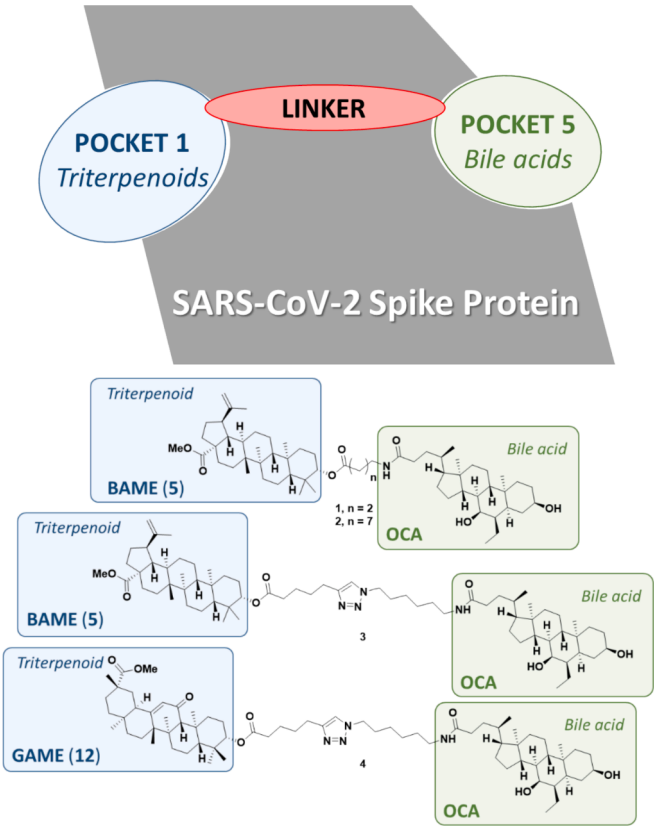

Fig. 2. Schematic representation of the designed bifunctional compounds **1–4.**

2. Results and discussion

2.1. Chemistry

The synthetic pathway for compounds **1–2** is depicted in Scheme 1.

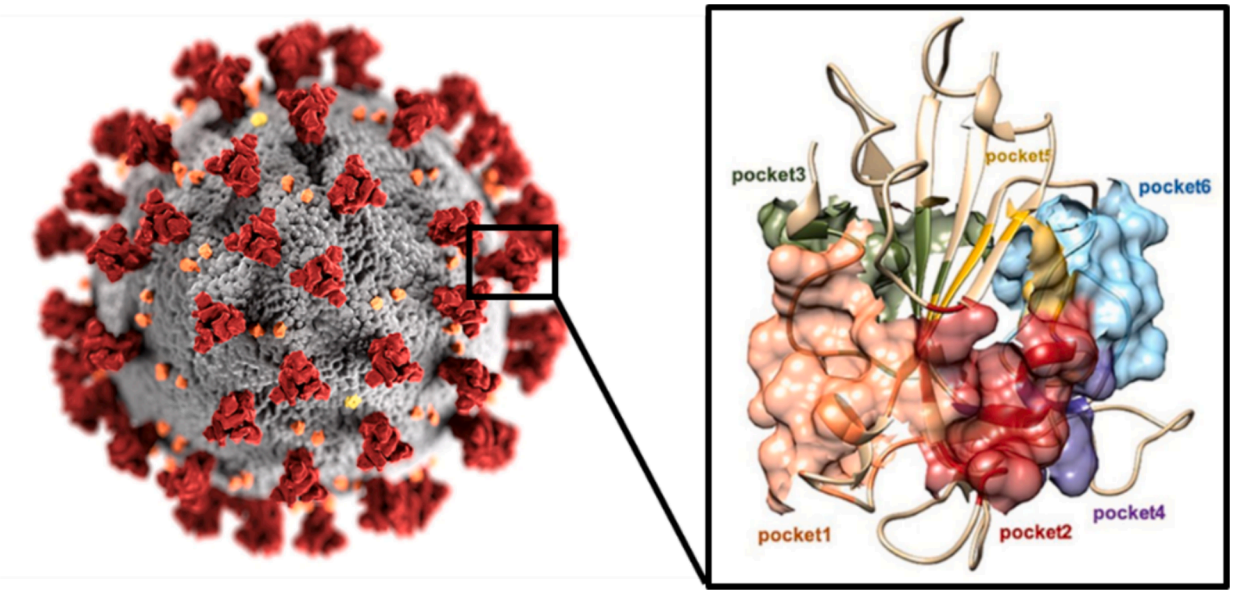

Fig. 1. Surface representation of six S/RBD pockets identified from virtual screening. Figure taken from Carino et al., licensed under CCBY.[13]

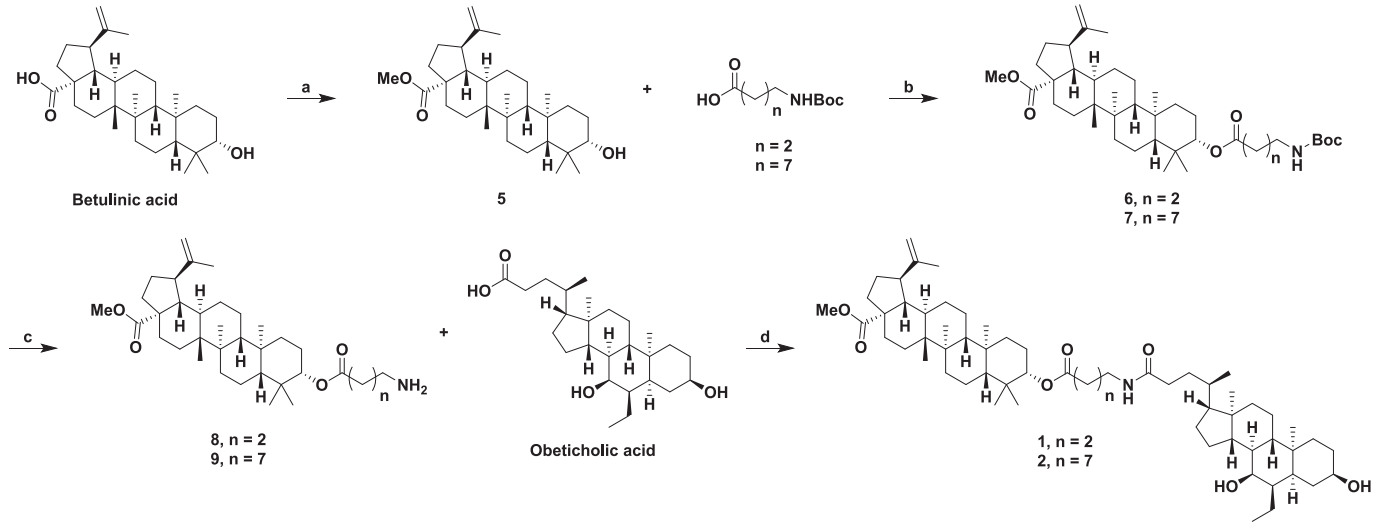

Scheme 1. Synthesis of **1–2**. Reagents and conditions: (a) $TMSCHN_2$, dry MeOH/toluene (2:3, *v/v*), rt, 4 h, 98 %; (b) EDCI, DMAP, TEA, dry DCM, 0 °C to 40 °C, 24 h, 86 % (**6**), 61 % (**7**); (c) HCl (4 M solution in 1,4–dioxane), dry 1,4–dioxane, 0 °C to rt, 8 h, 69 % (**8**), 71 % (**9**); (d) HATU, HOBt, DIPEA, dry DCM, rt, 3 h, 67 % (**1**), 67 % (**2**).

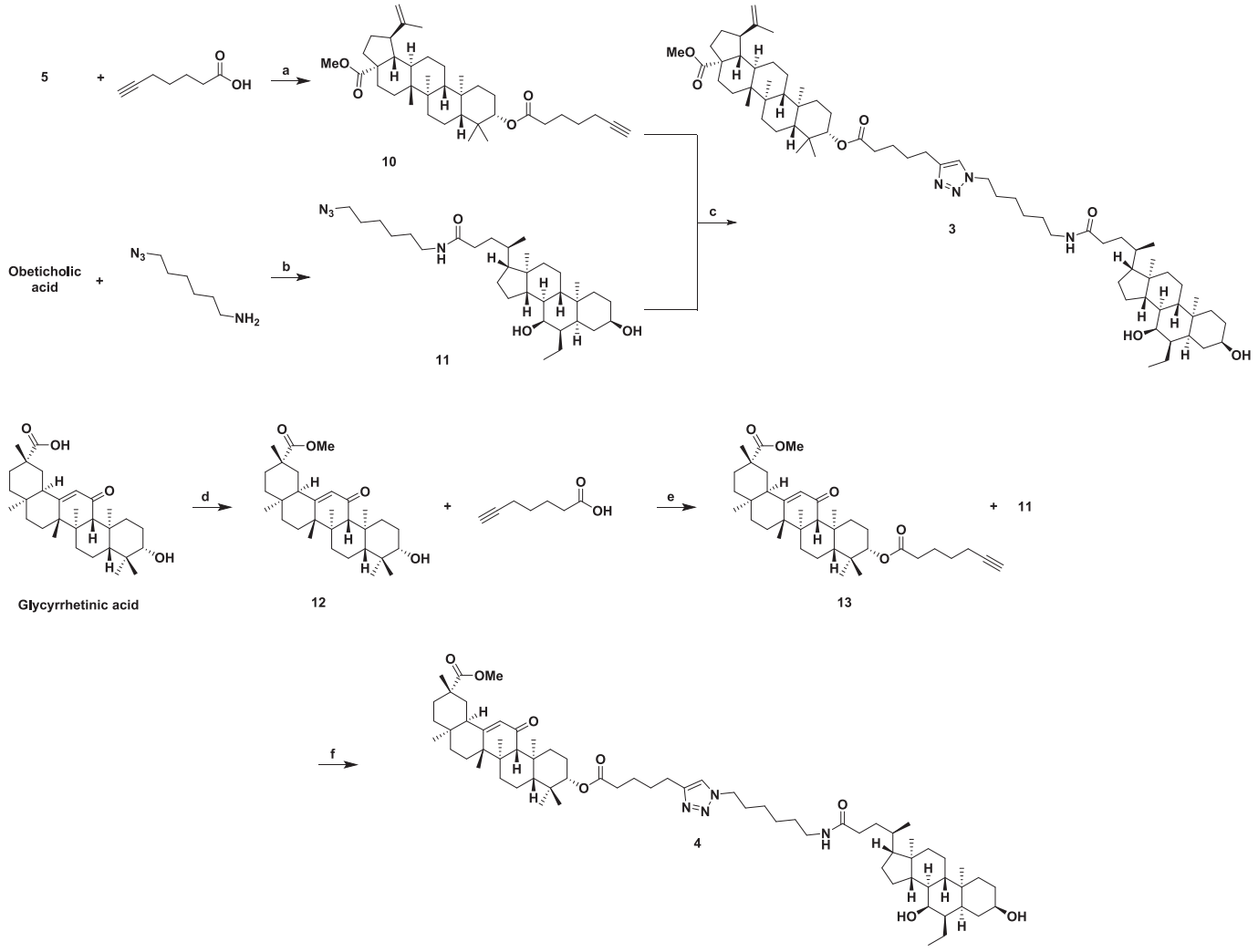

Scheme 2. Synthesis of **3–4.** Reagents and conditions: (a) EDCI, DMAP, TEA, dry DCM, rt, 24 h, 81 %; (b) EDCI, HOBt, NMM, dry DCM, 24 h, rt, 60 %; (c) $CuSO_4{\cdot}5H_2O$, sodium ascorbate, THF/H_2O (1:1, *v/v*), rt, 24 h, 61 %; (d) $TMSCHN_2$, dry MeOH/toluene (2:3, *v/v*), rt, 24 h, 63 %; (e) EDCI, DMAP, TEA, dry DCM, rt, 24 h, 49 %; (f) $CuSO_4{\cdot}5H_2O$, sodium ascorbate, THF/H_2O (1:1, *v/v*), rt, 24 h, 56 %.

Betulinic acid was converted into the corresponding methyl ester (BAME **5**) using an excess of $TMSCHN_2$ in a mixture of MeOH and toluene in quantitative yield. BAME was reacted with either γ-(Boc-amino)butyric acid or 9-Boc-amino-nonanoic acid in the presence of EDCI/DMAP as coupling agents, to afford intermediates **6** and **7** in good yield. Boc-deprotection with 4 M HCl in 1,4–dioxane of **6** and **7** provided γ-amino-butanoyl-BAME (**8**) and 9-amino-nonanoyl-BAME (**9**) in excellent yields. Finally, the target compounds butanoyl-BAME-OCA (**1**) and nonanoyl-BAME-OCA (**2**) were obtained in high yields by an amide formation reaction between γ-amino-butanoyl-BAME (**8**) or 9-amino-nonanoyl-BAME (**9**) with obeticholic acid (OCA), respectively, in the presence of HATU/HOBt as coupling agents.

The synthetic pathway for triazole-linked compounds **3–4** is depicted in Scheme 2. The approach used is based on a click reaction, linking an alkyne-functionalized BAME/GAME and obeticholic acid (OCA) functionalized with an azide through the formation of a triazole ring. BAME was reacted with 6-heptynoic acid in the presence of EDCI/DMAP as coupling agents to afford intermediate **10** in good yield. OCA was reacted with 6-azidohexan-1-amine in the presence of EDCI/HOBt as coupling agents to afford intermediate **11** in 60 % yield. A copper-catalyzed azide-alkyne cycloaddition (CuAAC) was performed between copmpounds **10** and **11** to provide final target compound **3** in good yield. A similar pathway was followed for the synthesis of **4**. Glycyrrhetinic acid was converted into its corresponding methyl ester (**GAME 12**) with an excess of $TMSCHN_2$ in a mixture of MeOH and toluene with the same procedure used for BAME. GAME, and then was reacted with 6-heptynoic acid in the presence of EDCI/DMAP as coupling agents to afford intermediate **13** in moderate yield. Similarly, a CuAAC was performed between compounds **11** and **13** to provide final target compound **4** in good yield. The structural confirmation and the purity determination for all synthesized compounds was achieved by ^{1}H NMR, ^{13}C NMR and HRMS; copies of the spectra are included in the Supporting information.

2.2. Docking

Molecular docking has been employed in order to investigate the interaction of bivalent compounds **1–4** with the S protein and the geometry of the bound complexes. First of all, BAME (**5**), GAME (**12**) and OCA were docked in their putative binding sites, previously identified by Carino et al.[13] Then, template docking was applied by restraining the BAME/GAME and OCA moieties in each bivalent compound **1–4** in the known binding geometries of their monomers, while allowing full relaxation of their amide- or triazole-based linkers. The nature of the linker connecting the two natural compounds primarily serves to position the two moieties in the favorable geometry, ensuring optimal interactions with the respective binding pockets. Additionally, the chemical composition of the linker itself could contribute to the overall affinity of the compound for the biological target by providing supplementary interactions. This dual role underscores the critical importance of linker in achieving both spatial alignment and enhanced binding efficiency. Bivalent compounds **1–4** were template-docked and subsequently, 2D interaction plots (Fig. S1 in Supplementary materials) were generated to study the specificity of the binding modes or bifunctional compounds (Fig. 3). Bivalent compounds **1** and **2**, incorporating an amide-based linker with 4- and 9-C atom chains, respectively, demonstrate the critical role of the linker in guiding interactions with the protein, primarily through hydrophobic interactions. The 4-C linker of compound **1** effectively positions the two natural moieties in a conformation that facilitates their binding within the S pockets (Fig. 3 – panel A). This precise spatial orientation underscores the significance of linker geometry in achieving functional engagement with the target. Notably, compound **2**, with its extended 9-C linker, further supports this binding through the establishment of a supplementary hydrogen bond between the amide NH group of the linker and Pro412 (Fig. 3 – panel B). This additional interaction not only reinforces the overall binding affinity but also provides a directional stabilization that improve the efficacy of the interaction. On the other hand, whenever a triazole spacer was incorporated in the linker, such moiety may establish π–π interactions with the amino acid residues of the S-RBD surface between pocket 1 and pocket 5, ideally achieving increased cooperative stabilization of the bound state of **3** and **4** bivalent compounds.[23] Compound **3** shows additional hydrophobic interactions provided by the presence of linker; in particular, the triazole moiety interacts with Val405 and its carbon

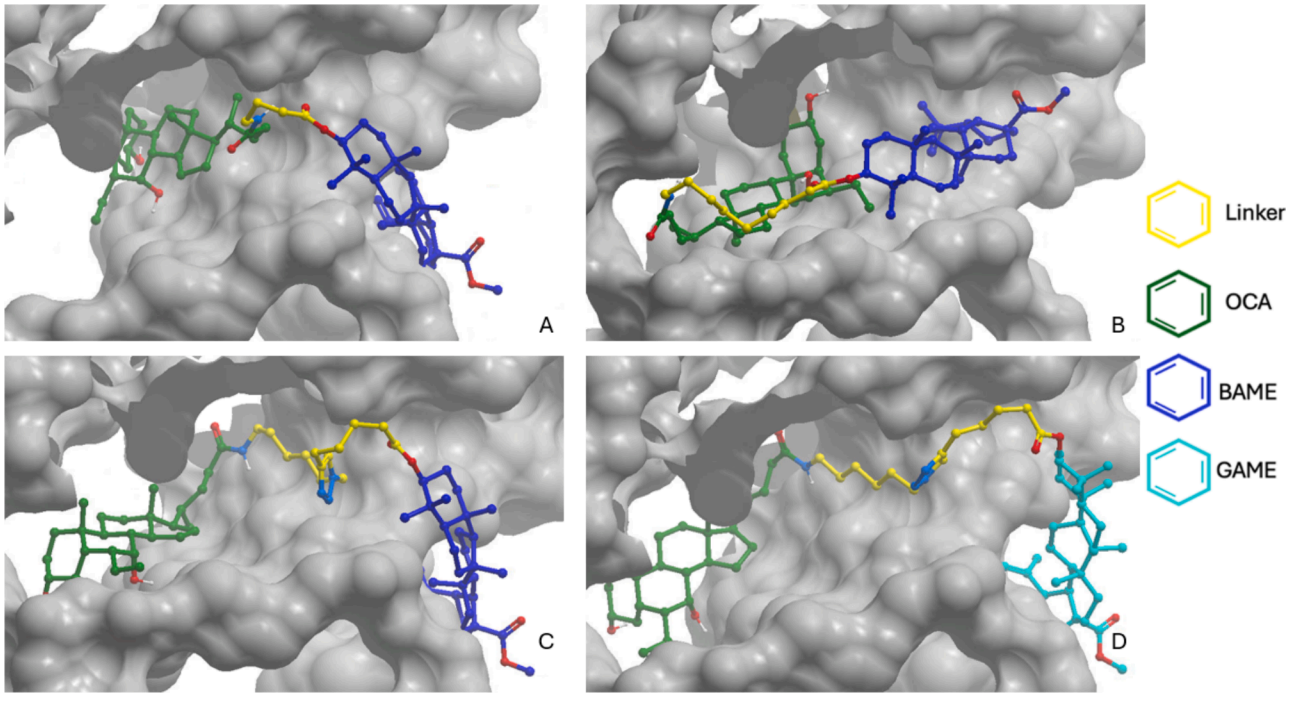

Fig. 3. Binding modes of the four bivalent targets **1–4**. Panel **A**: Shorter amide-linked BAME-OCA **1**; panel **B**: Longer amide-linked BAME-OCA **2**; panel **C**: Triazole-linked BAME-OCA **3**; panel **D**: triazole-linked GAME-OCA **4**.

chain with Ala435, Val510 and Ile402 (Fig. 3 – panel C). Lastly, compound **4**, once again, shows several hydrophobic interactions; in particular, its triazole ring interacts with Tyr495, while its carbon chain interacts with Leu452, Tyr453, Ile418, Asn422 and Val350 (Fig. 3 – panel D). The hydrophobic nature of the linkers serves as the primary driver of the interaction, while the specific hydrogen bond in molecule **2** offers additional stabilization. Detailed interactions are reported in Fig. S1 in Supplementary materials.

2.3. Compounds 1 and 2 specifically and effectively interfere with SARS-CoV-2 entry into ACE2 positive cells

Compounds **1–4** were subjected to bioassays using pseudotyped lentiviral particles where the native envelope glycoprotein of the lentivirus was replaced with the S protein of two different SARS-CoV-2 variants.[24] Bivalent compounds **1–4** were tested at a concentration of 10 μM, that was previously shown by Carino and co-workers to effectively reverse the binding between the SARS-CoV-2 Spike RBD and ACE2 in an *in vitro* assay for both BA, GA and OCA.[13] In addition, the same Authors showed that the incubation of the viral glycoprotein with the compounds before testing the ability of BA, GA and OCA of interfering with S/ACE2 binding increased their activity.[13] The experimental setting involves the transfection of human embryonic kidney (HEK) 293 T cells with a lentiviral backbone plasmid expressing the luciferase (Luc) reporter protein, along with a plasmid expressing the S protein and plasmids encoding essential lentiviral proteins required for HIV-based viral genome replication and particle assembly. Subsequently, transfected cells generate pseudotyped recombinant lentiviral particles (RLPs) suitable for infecting cells expressing hACE2, as the (HEK) 293 T-hACE cell line (Fig. 4). After their generation, pseudotyped RLPs are incubated with the bivalent compounds **1–4** for 1 h at 37 °C. Next, drug-treated pseudotyped RLPs are put in contact with target cells, initiating the process of viral entry into 293 T-hACE cells. Cells are maintained in medium containing 10 μM of the putative inhibitors. 48 h later, intracellular luciferase (Luc) expression is assayed by luminescence measurement.

In a first set of experiments, RLPs were pseudotyped with the envelope glycoprotein protein G of the Vesicular Stomatitis Virus (VSV). This glycoprotein efficiently pseudotypes RLPs, and can be used as a negative control for testing compounds' specificity of action. Cells were challenged with VSV-G-RLPs at the multiplicity of infection (MOI) of 1 Transducing Unit (TU)/cell, and of 0.1 TU/cell. In both cases, none of the compounds blocked viral entry (Fig. 5A), thus supporting their activity to be targeted on SARS-CoV-2 Spike. Next, the assay was conducted by using two SARS-CoV-2 S proteins, one bearing the D614G mutation and one derived from the Omicron sublineages, *i.e.* BA.2. Both RPLs were used at the MOI of 10 TU/cell, achieving in the untreated samples a level of Luc expression comparable to the one obtained for VSV-G-RPLs at the MOI of 0.1 TU/cell.

Betulinic acid (BA), glycyrrhetinic acid (GA) and OCA exhibited a modest and not statistically significant decrease in internalization of viral pseudotyped particles in overexpressing ACE2 293 T cells (HEK293T-hACE2), with comparable effects in the case of the D614G and Omicron S proteins (Fig. 5B, left and right respectively). In contrast, whereas triazole-based BAME-OCA **3** had a similar impact on viral internalization as free compounds in the case of the D614G S protein, it exhibited a significantly greater reduction when tested against the Omicron S protein (Fig. 5B). Conversely, triazole-based GAME-OCA **4** did not demonstrate a reduction in internalization for both S proteins (Fig. 5B). Importantly, bivalent alkylamide-linked compounds **1** and **2** displayed a consistent and statistically significant reduction in viral internalization in 293 T-hACE cells, both with the Omicron and D614G S protein variants (Fig. 5B).

3. Conclusions

In this work, we designed and synthesized bivalent compounds by linking pocket 1 ligands (BA and GA) with pocket 5 ligand OCA using variable linkers. The synthesis involved azide-alkyne click chemistry as well as amide and ester coupling reactions, resulting in bifunctional compounds possibly enhancing their antiviral potency by inhibiting activation of the SARS-CoV-2 recognition and internalization mechanism. This study evaluated the effects of such bivalent compounds on the internalization of pseudotyped viral particles in hACE2 expressing cells, with a focus on the D614G and Omicron variants. Specifically, bivalent alkyl-based compounds **1** and **2** consistently reduced viral internalization in both variants in two experimental replicates, highlighting their robust antiviral activity and revealing a dual mechanism of action, suggesting involvement beyond internalization and potentially affecting later stages of viral replication and dissemination. These results underline the critical role of linker design in optimizing compound interactions with biological targets, both through spatial orientation and complementary interactions. The multifaceted antiviral mechanism of **1** and **2** positions them as promising candidates to combat viral infections.

4. Materials and methods

4.1. Chemistry

Unless otherwise stated, reagents and solvents were purchased from

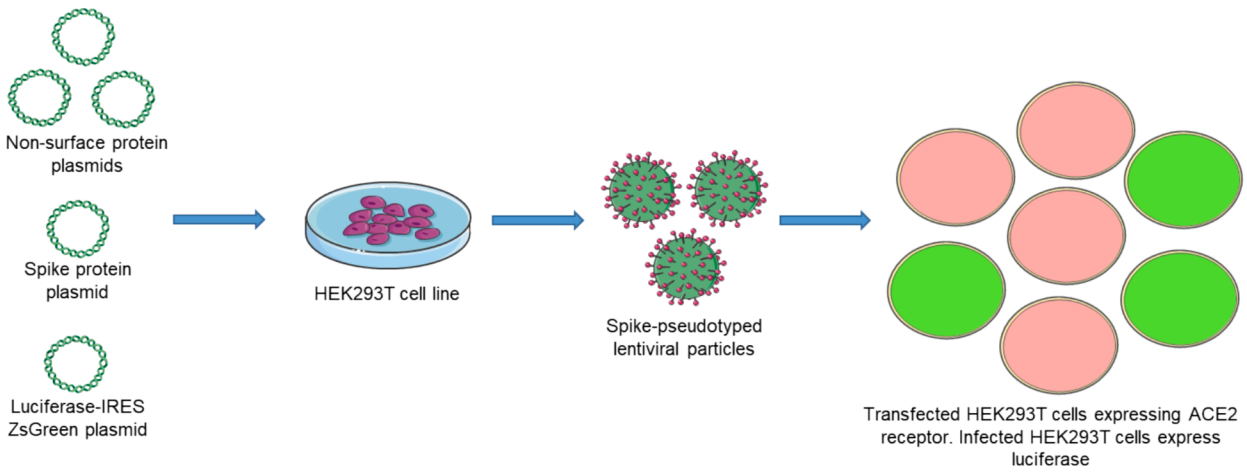

Fig. 4. General approach for lentiviral pseudotyping production in (HEK) 293 T cell lines. Transduced cells are depicted in green, as they express the reporter protein luciferase. (For interpretation of the references to colour in this figure legend, the reader is referred to the web version of this article.)

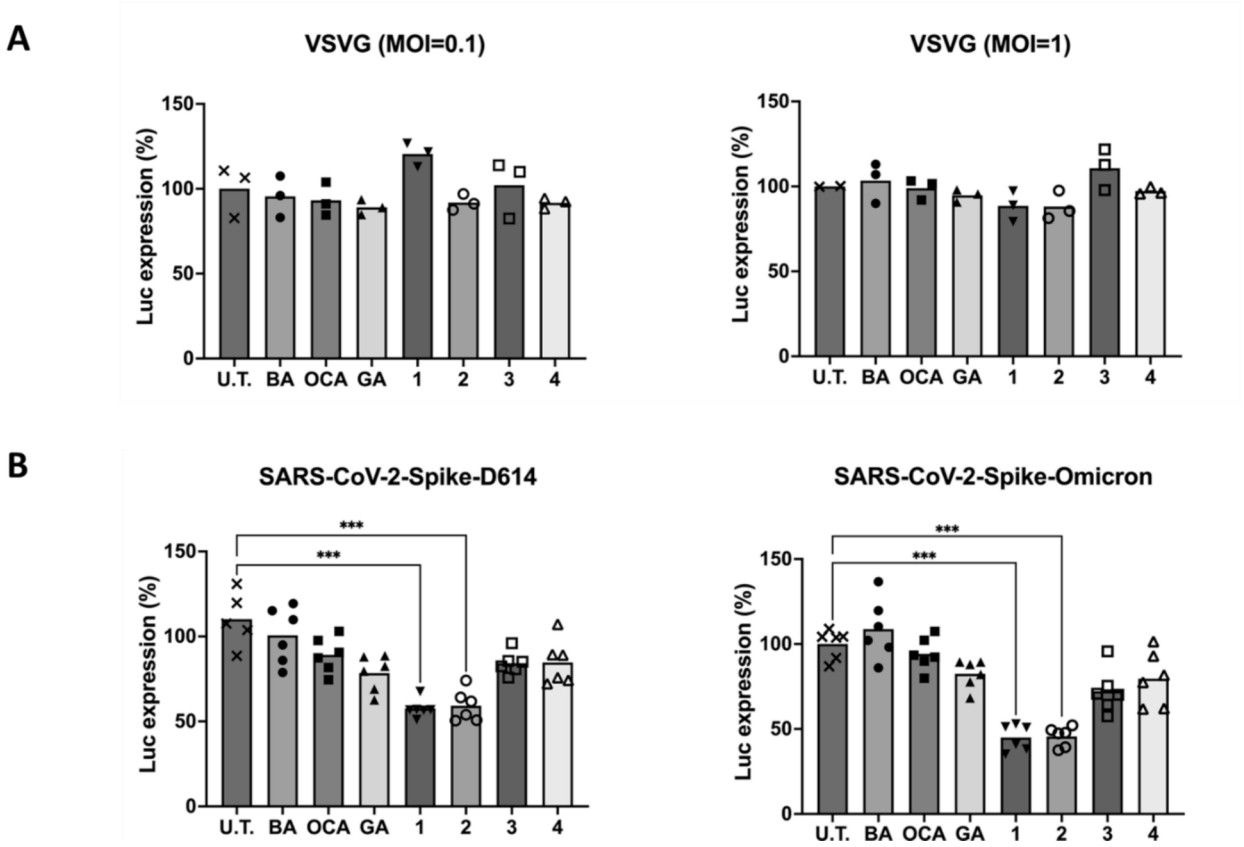

Fig. 5. Compounds **1** and **2** specifically reduce RLPs internalization into (HEK) 293 T-hACE cells. VSV-G (**A**) or D614G and Omicron S (**B**) pseudotyped RLPs were incubated with free natural compounds and bivalent targets **1–4** (10 μM) for 1 h at 37 °C. Next, (HEK) 293 T-hACE were challenged at the same concentration, and 48 h later luciferase (Luc) expression was evaluated. Graphs display the single values and the respective mean of the relative light units (RLUs) found for each experiment, expressed as percentages with respect to the results obtained for untreated (U.T.) cells. The data reported in B are from two replicates. Statistical analysis was performed by comparing the results obtained in the U.T. condition to the other with a Kruskal–Wallis test. *** highlight the statistically significant differences ($p < 0.001$).

Merck (Milan, Italy), Fluorochem (Hadfield, United Kingdom), TCI (Zwijndrecht, Belgium) or BLDPharm (Hamburg, Germany) and used without further purification. All reactions were carried out in oven-dried glass-ware, using dry solvents under nitrogen atmosphere and monitored by TLC on silica gel (Merck precoated 60 F_{254} plates), with detection by UV light (254 nm) or by permanganate or by molybdic reagent. Products were purified by flash column chromatography, using silica gel Merck 60 (230–400 mesh) as the stationary phase, or by a BIOTAGE® system in direct phase, using Biotage® Sfär Silica D cartridges (10/25 g). The elution method was as follows: flow 40–80 mL/min; equilibration time of 2/3 CV; monitoring wavelength: 254 nm, 280 nm; phases: *n*-hexane (HiPerSolv Chromanorm VWR *n*-hexane for HPLC-MS) (**A**), ethyl acetate (HiPerSolv Chromanorm VWR Ethyl acetate SuperGradient) (**B**). Purity of the final tested compounds was assured to be >95 % as assessed by NMR and HPLC analysis. ^{1}H NMR and ^{13}C NMR spectra were recorded at 298 K on a Brüker Avance Spectrometer (400 MHz), using commercially available deuterated solvents (Chloroform-*d*, MeOD). Chemical shifts are reported in parts per million (δ ppm), compared to TMS as an internal standard. Coupling constants (J) are given in hertz (Hz) and are quoted to the nearest 0.5 Hz. Peak multiplicities are described as follows: s, singlet; bs, broad singlet; d, doublet; m, multiplet; br, broad. High-resolution mass spectra (HRMS) were recorded using the Q-ToF Synapt G2-Si HDMS Acquity UPLC I-Class Photodiode Detector Array (PDA) (Waters). No unexpected or unusually high safety hazards were encountered.

4.2. Cells

The human embryonic kidney HEK293T (ATCC CRL-3216™) cell line was purchased from the American Type Culture Collection (ATCC); the HEK-293 T-hACE (NR-5211) cell line was obtained from the Biodefense and Emerging Infections Research Resources (BEI). Cells were maintained in Dulbecco's Modified Eagle Medium (DMEM) supplemented with 10 % (v/v) fetal bovine serum (FBS) (Thermofisher Scientific). All cell lines were grown at 37 °C in a humidified atmosphere with 5 % CO_2.

4.3. Generation and titration of pseudotyped recombinant lentiviral particles

Pseudotyped recombinant lentiviral particles were generated through calcium phosphate transfection of HEK293T cells. Specifically, 2.5×10^6 HEK293T cells were seeded on 10 cm Petri dishes and allowed to grow for 16–24 h until reaching approximately 80 % confluence. Next, cells were cotransfected with the following plasmids: 10 μg of the HIV-1-based lentiviral vector containing a CMV promoter to drive expression of luciferase followed by an internal ribosome entry site (IRES) and ZsGreen (BEI NR-52516) along with 2.2 μg each of plasmids HDM-Hgpm2 (BEI, NR-52517), pRC-CMV-Rev1b (BEI NR-52519), HDM-tat1b (BEI NR-52518) and 3.4 μg of the plasmid encoding for the appropriate envelope glycoprotein (either the SARS-CoV-2 Spike D614G BEI NR-53765, or the spike Omicron BA.2 lineage that was synthesized and then cloned into the same plasmid backbone, or the glycoprotein G of the VSV pMD2.VSV.G, kindly provided by L. Naldini

(San Raffaele Telethon Institute for Gene Therapy, Milan, Italy). 24 h post-transfection, cells were washed with phosphate buffer solution (PBS 1X, pH 7.4) and maintained in DMEM 10 %. At 60 h post-transfection, cell culture media (supernatants) containing the recombinant lentiviral particles (RLPs) were harvested, filtered with a 0.45-μm-pore-size membrane and stored at −80 °C until use. RLPs were titrated with an HIV-1 p24 ELISA kit (XpressBio, Frederick, MD, USA), following manufacturer's instructions. This assay measures the p24 antigen concentration (pg/mL), and thus indirectly the number of viral particles in the sample. Briefly, cell supernatants were serially diluted and 200 μL of sample dilutions (1:100, 1:1000 and 1:10,000) were loaded onto an ELISA plate and tested in duplicate. These dilutions were found empirically to yield absorbance values in the range of the standard curve. The positive control (200 pg/mL) was supplied from the kit and diluted (2× dilution factor) in 10 % DMEM. Upon adding the lysis reagent, samples were incubated at 37 °C for 1 h. Next, the substrate solution was added and, 10 min later, a stop solution was added in each well. The absorbance was immediately read at 450 nm using a microtitration plate reader and data were analyzed using Excel software. A standard curve was generated, accepting R^2 values $\geq$ 0.95, and the transducing units per ml (TU/mL) were calculated by adopting the formula:

$$\text{Titer}\,(\text{TU/mL}) = \frac{\text{A450} - \text{b}}{\text{m}} * 100 * \text{dilution factor}$$

where b and m are the coefficients of the standard curve (y = mx + b).

4.4. Viral internalization assay

Single-round recombinant HIV-1 pseudotyped by the different envelope glycoproteins were adopted to measure the ability of bivalent compounds **1**–**4** to inhibit virus entry into ACE2 expressing cells. The recombinant viruses were incubated with each compound (final concentration of 10 μM in DMEM 10 % FBS, from a 100 mM stock solution in DMSO) for 1 h at 37 °C, and then used to transduce (HEK) 293 T-hACE2 cells (12500 cells/well in a 96 well plate). Cells were maintained in DMEM 10 % FBS containing 10 μM of compounds **1–4**. 48 h later, the luciferase activity was measured by using the Bright-Glo Luciferase Assay System (E2610, Promega, Madison, WI, USA) following the manufactory's protocol. In details, 100 μL of Bright-Glo™ Reagent was added to each well and incubated for 2 min at room temperature. Samples were tested in triplicate. The luminescence was determined using a VICTOR X2 Multilabel Plate Reader (PerkinElmer, Waltham, MA, USA) with no attenuation and a luminescence integration time of 1 s.

4.5. Docking

The crystal structure of the SARS-CoV-2 Spike protein was obtained from the Protein Data Bank, (PDB ID: 7DZW).[25] As input files for BAME, GAME and OCA their 3D conformations were downloaded from PubChem and lastly, for bifunctional compounds **1–4** their SMILES were used. ICM-Pro 3.9–4 was used for both input files' preparation and docking simulations.[26] Docking has been performed with biased probability Monte Carlo (BPMC) procedure and on global optimization of the flexible ligand, and a weighted scoring function has been employed.[27,28] Docking thoroughness was increased to 10.0 and 100 conformations were generated; all remaining settings were left to default values. The docked conformations were used as a template for the docking of the bifunctional compounds. The 'Fuzzy' method, a template docking technique implemented in ICM-Pro was used to dock bivalent compounds **1–4**. They were docked with spatial arrangement constraints based on the conformations generated by the docking of BAME, GAME and OCA, and were generated by combining one triterpene and a bile acid separated by a linker. 2D interactions have been calculated using ICM-Pro with default settings.

4.6. Spectral and characterization data

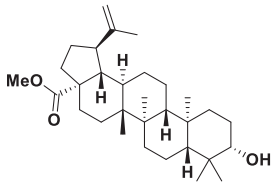

BAME (5): Trimethylsilyldiazomethane (2.0 M in *n*-hexane, 985 μL, 1.97 mmol, 1.5 equiv) was added dropwise to a solution of betulinic acid (600 mg, 1.31 mmol, 1.0 equiv) in dry MeOH/toluene 2:3 (27 mL, *v/v*). The reaction mixture was stirred at rt for 4 h. Et_2O (24 mL) and 17 % acetic acid solution in water (21 mL) were added, then the resulting suspension was extracted with Et_2O (3 × 20 mL). The collected organic phases were dried over Na_2SO_4 and concentrated under reduced pressure, affording pure **5** with 98 % yield (602 mg) as a white solid without any further purification. ^{1}H NMR (400 MHz, Chloroform-*d*): δ 4.73 (s, 1H), 4.60 (s, 1H), 3.67 (s, 3H), 3.18 (dd, J = 11.3, 4.9 Hz, 1H), 2.99 (td, J = 11.0, 4.5 Hz, 1H), 2.30–2.13 (m, 2H), 1.95–1.82 (m, 2H), 1.68 (s, 5H), 1.63–1.46 (m, 6H), 1.46–1.30 (m, 9H), 1.30–1.20 (m, 3H), 0.96 (s, 6H), 0.91 (s, 3H), 0.82 (s, 3H), 0.75 (s, 3H), 0.67 (d, J = 9.0 Hz, 1H). ^{13}C NMR (100 MHz, Chloroform-*d*): δ 177.1, 151.0, 110.0, 79.4, 57.0, 55.8, 51.7, 51.0, 49.9, 47.4, 42.8, 41.1, 39.3, 39.2, 38.7, 37.6, 37.4, 34.8, 32.6, 31.1, 30.1, 28.4, 27.9, 26.0, 21.3, 19.8, 18.8, 16.6, 16.4, 15.8, 15.2. $[\alpha]_D^{20}$ = +4.0000 ± 0.2093 in Chloroform. MS (ESI), *m/z* [M + Na]$^+$: 493.66. HRMS (ESI), *m/z* [M + H]$^+$: calculated for $C_{31}H_{51}O_3^+$471.3833; found 471.3847.

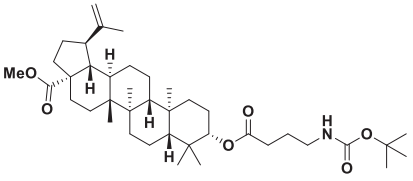

9-Boc-amino-butanoyl-BAME (6): EDCI (169 mg, 0.88 mmol, 2.1 equiv), DMAP (26 mg, 0.21 mmol, 0.5 equiv) and TEA (123 μL, 0.88 mmol, 2.1 equiv) were added to a solution of γ-(Boc-amino)butyric acid (203 mg, 0.67 mmol, 1.6 equiv) in dry DCM (4 mL) at 0 °C. The reaction mixture was left stirring at rt for 20 min, then **BAME (5)** (200 mg, 0.42 mmol, 1.0 equiv) was added. The mixture was stirred at 40 °C for 24 h, then saturated NH_4Cl solution (10 mL) was added. The aqueous phase was extracted with DCM (3 × 20 mL), then the collected organic phases were dried over Na_2SO_4, and concentrated under reduced pressure. Compound **6** was obtained with 86 % yield (238 mg) as a whitish solid after automatic flash column chromatography purification (from 95:5 to 6:4*n*-hexane/ethyl acetate *v/v* as eluent). ^{1}H NMR (400 MHz, Chloroform-*d*): δ 4.73 (d, J = 2.3 Hz, 1H), 4.60 (d, J = 1.0 Hz, 1H), 4.51–4.44 (m, 1H), 3.66 (s, 3H), 3.16 (q, J = 6.6 Hz, 2H), 2.99 (td, J = 10.9, 4.4 Hz, 1H), 2.34 (t, J = 7.4 Hz, 2H), 2.26–2.15 (m, 2H), 1.94–1.76 (m, 4H), 1.68 (s, 4H), 1.66–1.51 (m, 6H), 1.43 (s, 10*H*), 1.41–1.31 (m, 8H), 1.30–1.02 (m, 4H), 0.96 (s, 3H), 0.91 (s, 3H), 0.88–0.73 (m, 10*H*). ^{13}C NMR (100 MHz, Chloroform-*d*): δ 176.8, 173.2, 156.1, 150.7, 109.8, 81.2, 79.3, 56.7, 55.6, 51.4, 50.6, 49.6, 47.1, 42.5, 40.8, 40.2, 38.5, 38.4, 38.0, 37.2, 37.1, 34.4, 32.3, 32.2, 30.7, 29.8, 28.5 (3C), 28.1, 25.6, 25.5, 23.9, 21.0, 19.5, 18.3, 16.7, 16.3, 16.1, 14.8. $[\alpha]_D^{20}$ = +11.2057 ± 0.2949 in Chloroform. MS (ESI), *m/z* [M + Na]$^+$: 678.71. HRMS (ESI), *m/z* [M + H]$^+$: calculated for $C_{40}H_{66}NO_6^+$656.4885; found 656.4869.

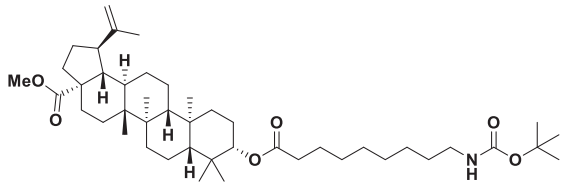

9-Boc-amino-nonanoyl-BAME (7): EDCI (257 mg, 1.34 mmol, 2.1 equiv), DMAP (39 mg, 0.32 mmol, 0.5 equiv) and TEA (187 μL, 1.34 mmol, 2.1 equiv) were added to a solution of 9-Boc-amino-nonanoic acid (279 mg, 1.02 mmol, 1.6 equiv) in dry DCM (6 mL) at 0 °C. The reaction mixture was left stirring for at rt 20 min, then **BAME (5)** (300 mg, 0.64 mmol, 1.0 equiv) was added. The reaction mixture was stirred at 40 °C for 24 h, then saturated NH_4Cl solution (10 mL) was added. The aqueous phase was extracted with DCM (3 × 20 mL), then the collected organic phases were dried over Na_2SO_4 and concentrated under reduced pressure. Compound **7** was obtained with 61 % yield (265 mg) as a whitish solid after flash column chromatography purification (8:2*n*-hexane/ethyl acetate *v/v* as eluent). ^{1}H NMR (400 MHz, Chloroform-*d*): δ 4.73 (s, 1H), 4.59 (s, 1H), 4.46 (dd, J = 10.5, 5.8 Hz, 1H), 3.66 (s, 3H), 3.09 (q, J = 6.8 Hz, 2H), 2.98 (dt, J = 10.9, 5.5 Hz, 1H), 2.32–2.13 (m, 4H), 1.95–1.84 (m, 2H), 1.68 (s, 5H), 1.62 (s, 6H), 1.43 (s, 12H), 1.41–1.20 (m, 18H), 1.15 (td, J = 11.6, 2.5 Hz, 1H), 0.95 (s, 5H), 0.91 (s, 3H), 0.83 (d, J = 5.1 Hz, 10*H*). ^{13}C NMR (100 MHz, Chloroform-*d*): δ 176.7, 173.7, 155.9, 150.6, 109.7, 80.7, 79.0, 56.6, 55.5, 51.3, 50.6, 49.6, 47.1, 42.5, 40.8, 40.7, 38.5, 38.3, 37.9, 37.2, 37.0, 34.9, 34.4, 32.3, 30.7, 30.1, 29.8, 29.3, 29.2, 29.2, 28.5 (3C), 28.1, 26.8, 25.6, 25.2, 23.8, 21.0, 19.4, 18.3, 16.7, 16.3, 16.0, 14.8. $[\alpha]_D^{20}$ = +10.6124 ± 0.0943 in Chloroform. MS (ESI), *m/z* $[M + Na]^+$: 748.85. HRMS (ESI), *m/z* $[M + H]^+$: calculated for $C_{45}H_{76}NO_6^+$726.5667; found 726.5651.

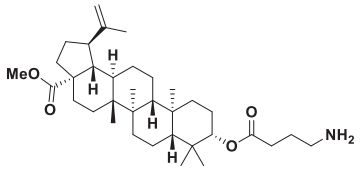

9-amino-butanoyl-BAME (8): HCl in 1,4-dioxane (4.0 M, 264 μL, 1.05 mmol, 7 equiv) was added dropwise to a solution of **6** (100.0 mg, 0.15 mmol, 1.0 equiv) in dry 1,4-dioxane (1.5 mL) cooled at 0 °C. The reaction mixture was left stirring at rt for 8 h, then concentrated under reduced pressure. The resulting solid was dissolved in DCM (10 mL) and washed with saturated Na_2CO_3 solution (10 mL), then the aqueous phase was extracted with DCM (3 × 20 mL) and the collected organic phases were dried over Na_2SO_4 and concentrated under reduced pressure. Compound **8** was obtained with 69 % yield (57 mg) as a white solid after flash column chromatography purification (from 99:1 to 9:1 DCM/MeOH *v/v* as eluent). ^{1}H NMR (400 MHz, Chloroform-*d*): δ 4.73 (s, 1H), 4.59 (s, 1H), 4.47 (dd, J = 10.3, 6.1 Hz, 1H), 3.66 (s, 3H), 2.98 (td, J = 11.0, 4.5 Hz, 1H), 2.75 (t, J = 7.0 Hz, 2H), 2.36 (t, J = 7.4 Hz, 2H), 2.26–2.14 (m, 2H), 1.93 (s, 3H), 1.90–1.74 (m, 5H), 1.68 (s, 3H), 1.65–1.53 (m, 3H), 1.51–1.30 (m, 9H), 1.29–1.19 (m, 3H), 1.18–0.99 (m, 2H), 0.95 (s, 3H), 0.91 (s, 3H), 0.86–0.81 (m, 9H), 0.81–0.75 (m, 1H). ^{13}C NMR (100 MHz, Chloroform-*d*): δ 177.1, 173.4, 151.0, 110.1, 81.7, 57.0, 55.9, 51.7 (2C), 50.9, 49.9, 47.5, 42.9, 41.2, 41.1, 38.9, 38.7, 38.3, 37.6, 37.4, 34.7, 32.6, 32.4, 31.1, 30.2, 28.5, 25.9, 24.2, 21.4, 19.8, 18.6, 17.0, 16.6, 16.4, 15.2. $[\alpha]_D^{20}$ = +11.9635 ± 0.0906 in Chloroform. MS (ESI), *m/z* $[M + H]^+$: 556.47. HRMS (ESI), *m/z* $[M + H]^+$: calculated for $C_{35}H_{58}NO_4^+$556.4360; found 556.4376.

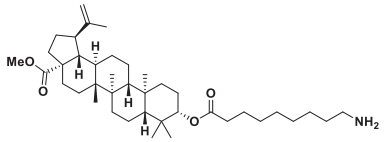

9-amino-nonanoyl-BAME (9): HCl in 1,4-dioxane (4.0 M, 140 μL, 0.56 mmol, 8 equiv) was added dropwise to a solution of **7** (50.0 mg, 0.07 mmol, 1.0 equiv) in dry 1,4-dioxane (700 μL) cooled at 0 °C. The reaction mixture was left stirring at rt for 8 h, then concentrated under reduced pressure. The resulting solid was dissolved in DCM (10 mL) and washed with saturated Na_2CO_3 solution (10 mL), then the aqueous phase was extracted with DCM (3 × 20 mL) and the collected organic phases were dried over Na_2SO_4 and concentrated under reduced pressure. Compound **9** was obtained with 71 % yield (34 mg) as a white solid after flash column chromatography purification (from 98:2 to 9:1 DCM/MeOH *v/v* as eluent). ^{1}H NMR (400 MHz, Chloroform-*d*): δ 4.73 (s, 1H), 4.59 (s, 1H), 4.46 (dd, J = 10.3, 6.0 Hz, 1H), 3.66 (s, 3H), 2.98 (td, J = 10.9, 4.5 Hz, 1H), 2.72 (t, J = 7.2 Hz, 2H), 2.57 (s, 4H), 2.32–2.11 (m, 4H), 1.94–1.80 (m, 2H), 1.68 (s, 3H), 1.66–1.54 (m, 4H), 1.53–1.44 (m, 3H), 1.44–1.23 (m, 19H), 1.21–1.00 (m, 2H), 0.95 (s, 4H), 0.91 (s, 3H), 0.86–0.72 (m, 10*H*). ^{13}C NMR (100 MHz, Chloroform-*d*): δ 176.8, 173.7, 150.6, 109.7, 80.7, 56.7, 55.5, 53.0, 51.7, 51.4, 50.6, 49.6, 47.1, 42.5, 41.9, 40.8, 38.5, 38.4, 37.9, 37.2, 37.1, 34.9, 34.4, 32.3, 30.7, 29.8, 29.3, 29.2, 28.1, 26.9, 25.6, 25.2, 23.9, 21.0, 19.5, 18.3, 16.7, 16.3, 16.1, 14.8. $[\alpha]_D^{20}$ = +10.3347 ± 0.7288 in Chloroform. MS (ESI), *m/z* $[M + H]^+$: 626.73. HRMS (ESI), *m/z* $[M + H]^+$: calculated for $C_{40}H_{68}NO_4^+$626.5143; found 626.5157.

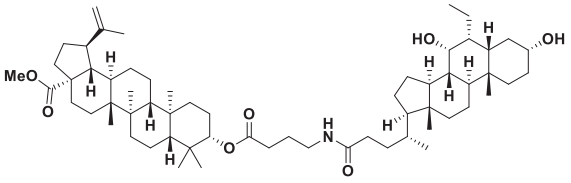

Butanoyl-BAME-OCA (1): HATU (27 mg, 0.07 mmol, 1.1 equiv), HOBt (4 mg, 0.03 mmol, 0.5 equiv), DIPEA (16 μL, 0.09 mmol, 1.5 equiv) and **8** (32 mg, 0.06 mmol, 1.0 equiv) were added to a solution of obeticholic acid (29 mg, 0.07 mmol, 1.1 equiv) in dry DCM (600 μL). The mixture was stirred at rt for 3 h, then saturated NH_4Cl solution (10 mL) was added. The aqueous phase was extracted with DCM (3 × 20 mL), then the collected organic phases were dried over Na_2SO_4 and concentrated under reduced pressure. Compound **1** was obtained with 67 % yield (41 mg) as a whitish solid after flash column chromatography purification (from 1:1 to 1:9*n*-hexane/ethyl acetate *v/v* as eluent). ^{1}H NMR (400 MHz, Chloroform-*d*): δ 5.78 (t, J = 6.2 Hz, 1H), 4.72 (s, 1H), 4.58 (s, 1H), 4.46 (t, J = 8.1 Hz, 1H), 3.73–3.60 (m, 4H), 3.38 (dt, J = 10.9, 5.9 Hz, 1H), 3.27 (q, J = 6.7 Hz, 2H), 2.98 (t, J = 10.4 Hz, 1H), 2.78 (s, 3H), 2.33 (t, J = 7.2 Hz, 2H), 2.27–2.13 (m, 2H), 2.10–1.98 (m, 1H), 1.97–1.72 (m, 9H), 1.67 (s, 6H), 1.62–1.53 (m, 3H), 1.52–1.22 (m, 28H), 1.18–1.09 (m, 4H), 1.05–0.98 (m, 2H), 0.94 (s, 3H), 0.92 (s, 2H), 0.90 (s, 4H), 0.88 (s, 3H), 0.85–0.79 (m, 9H), 0.79–0.73 (m, 1H), 0.64 (s, 3H). ^{13}C NMR (100 MHz, Chloroform-*d*): δ 176.7, 173.7, 173.4, 150.6, 109.7, 81.3, 72.4, 70.9, 56.7, 56.0, 55.6, 51.3, 50.6, 50.6, 49.6, 47.1, 45.4, 42.9, 42.5, 41.4, 40.8, 40.2, 39.8, 39.1, 38.5, 38.4, 38.0, 37.2, 37.1, 35.7, 35.6, 35.6, 34.4, 34.1, 33.7, 33.4, 32.4, 32.3, 31.9, 30.8, 30.7, 29.8, 28.3, 28.1, 25.6, 24.9, 23.9, 23.8, 23.3, 22.4, 21.0, 20.9, 19.5, 18.5, 18.3, 16.7, 16.3, 16.1, 14.8, 11.9, 11.8. $[\alpha]_D^{20}$ = +8.6856 ± 0.2216 in Chloroform. MS (ESI), *m/z* $[M + Na]^+$: 980.99. HRMS (ESI), *m/z* $[M + Na]^+$: calculated for $C_{61}H_{99}NNaO_7^+$980.7314; found 980.7322.

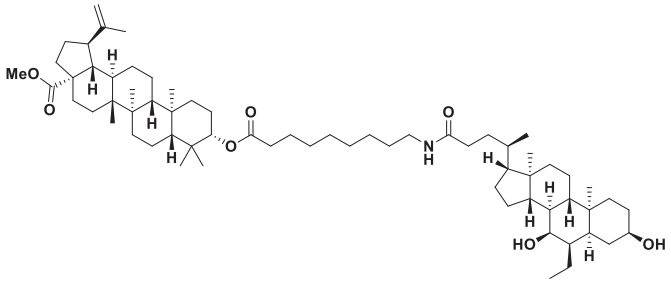

Nonanoyl-BAME-OCA (2): HATU (27 mg, 0.07 mmol, 1.1 equiv), HOBt (4 mg, 0.03 mmol, 0.5 equiv), DIPEA (16 μL, 0.09 mmol, 1.5 equiv) and **9** (38 mg, 0.06 mmol, 1.0 equiv) were added to a solution of obeticholic acid (29 mg, 0.07 mmol, 1.1 equiv) in dry DCM (600 μL). The mixture was stirred at rt for 3 h, then saturated NH_4Cl solution (10 mL) was added. The aqueous phase was extracted with DCM (3 × 20 mL), then the collected organic phases were dried over Na_2SO_4 and concentrated under reduced pressure. Compound **2** was obtained with 67 % yield (37 mg) as a whitish solid after flash column chromatography purification (from 1:1 to 1:9*n*-hexane/ethyl acetate *v/v* as eluent). ^{1}H NMR (400 MHz, Chloroform-*d*): δ 5.45 (t, J = 5.2 Hz, 1H), 4.72 (s, 1H), 4.59 (s, 1H), 4.46 (dd, J = 9.9, 6.3 Hz, 1H), 3.69 (s, 1H), 3.65 (s, 3H), 3.47 (s, 1H), 3.45–3.33 (m, 3H), 3.21 (q, J = 6.6 Hz, 2H), 2.98 (td, J = 11.1, 4.8 Hz, 1H), 2.79 (s, 3H), 2.30–2.14 (m, 6H), 2.10–1.99 (m, 3H), 1.99–1.72 (m, 12H), 1.72–1.53 (m, 17H), 1.53–1.22 (m, 26H), 1.21–1.09 (m, 3H), 1.07–0.98 (m, 2H), 0.95 (s, 3H), 0.93 (s, 1H), 0.91 (s, 4H), 0.88 (s, 3H), 0.85–0.81 (m, 9H), 0.80–0.75 (m, 1H), 0.65 (s, 3H). ^{13}C NMR (101 MHz, Chloroform-*d*): δ 176.8, 173.8, 173.5, 150.7, 109.7, 80.8, 72.5, 71.0, 56.7, 56.0, 55.6, 51.4, 50.7, 50.6, 49.6, 47.1 (2C), 45.4, 42.9, 42.5, 41.4, 40.8, 40.2, 39.8, 39.6, 38.5, 38.4, 38.0, 37.3, 37.1, 35.7, 35.6, 34.9, 34.4, 34.1, 33.8, 33.4, 32.3, 32.0, 30.8 (2C), 29.8 (2C), 29.2, 29.2, 28.4, 28.1, 26.9, 25.6, 25.2, 23.9 (2C), 23.3, 22.4, 21.0, 20.9, 19.5, 18.5, 18.3, 16.7, 16.3, 16.1, 14.8, 11.9, 11.8. $[\alpha]_D^{20}$ = +7.7158 ± 0.2683 in Chloroform. MS (ESI), *m/z* $[M + Na]^+$: 1050.90. HRMS (ESI), *m/z* $[M + Na]^+$: calculated for $C_{66}H_{109}NNaO_7^+$1050.8096; found 1050.8080.

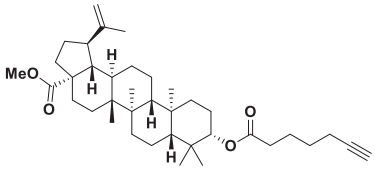

6-alkyne-heptyl-BAME (10): EDCI (85 mg, 0.44 mmol, 2.1 equiv), DMAP (13 mg, 0.11 mmol, 0.5 equiv), TEA (60 μL, 0.44 mmol, 2.1 equiv) and **BAME (5)** (100 mg, 0.21 mmol, 1.0 equiv) were added to a solution of 6-heptynoic acid (43 μL, 0.37 mmol, 1.6 equiv) in dry DCM (700 μL). The mixture was stirred at rt for 24 h, then saturated NH_4Cl solution (10 mL) was added. The aqueous phase was extracted with DCM (3 × 20 mL), then the collected organic phases were dried over Na_2SO_4 and concentrated under reduced pressure. Compound **10** was obtained with 81 % yield (98 mg) as a whitish solid after flash column chromatography purification (9:1*n*-hexane/ethyl acetate *v/v* as eluent). ^{1}H NMR (400 MHz, MeOD): δ 4.76–4.72 (m, 1H), 4.62 (dq, J = 2.8, 1.4 Hz, 1H), 4.48 (dd, J = 11.0, 5.3 Hz, 1H), 3.68 (s, 3H), 3.07–2.96 (m, 1H), 2.40–2.32 (m, 2H), 2.31–2.23 (m, 3H), 2.22 (s, 2H), 1.96–1.82 (m, 2H), 1.78–1.74 (m, 2H), 1.72–1.71 (m, 3H), 1.68–1.37 (m, 16H), 1.35–1.07 (m, 4H), 1.04 (s, 4H), 0.97 (s, 3H), 0.93–0.91 (m, 3H), 0.89 (s, 3H), 0.88 (s, 3H), 0.87–0.83 (m, 1H). ^{13}C NMR (100 MHz, MeOD): δ 176.7, 173.7, 150.4, 108.9, 83.1, 81.0, 68.4, 56.5, 55.5, 50.5, 50.4, 49.3, 47.1, 42.2, 40.5, 38.3, 38.2, 37.5, 36.9, 36.5, 34.1, 33.6, 31.7, 30.2, 29.4, 27.7, 27.2, 25.4, 23.9, 23.4, 20.7, 18.2, 17.9, 17.3, 15.7, 15.4, 15.2, 13.8. $[\alpha]_D^{20}$ = +16.9038 ± 0.7260 in Chloroform. MS (ESI), *m/z* $[M + Na]^+$: 601.42. HRMS (ESI), *m/z* $[M + H]^+$: calculated for $C_{38}H_{59}O_4^+$579.4408; found 579.4420.

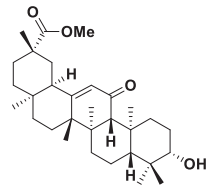

GAME (12): Trimethylsilyldiazomethane (2.0 M in *n*-hexane, 550 μL, 1.10 mmol, 2.0 equiv) was added dropwise to a solution of glycyrrhetinic acid (260 mg, 0.55 mmol, 1.0 equiv) in dry MeOH/toluene 2:3 (12 mL, *v/v*). The reaction mixture was stirred at rt for 24 h. Et_2O (24 mL) and 10 % acetic acid solution in water (10 mL) were added, then the resulting suspension was extracted with Et_2O (3 × 20 mL) and the collected organic phases were dried over Na_2SO_4 and concentrated under reduced pressure. Compound **12** was obtained with 63 % yield (168 mg) as a white solid after flash column chromatography purification (8:2*n*-hexane/ethyl acetate *v/v* as eluent). ^{1}H NMR (400 MHz, Chloroform-*d*): δ 5.66 (s, 1H), 3.69 (s, 3H), 3.22 (dd, J = 10.7, 5.6 Hz, 1H), 2.79 (dt, J = 13.5, 3.6 Hz, 1H), 2.34 (s, 1H), 2.08 (ddd, J = 13.7, 4.5, 1.9 Hz, 1H), 2.04–1.97 (m, 2H), 1.91 (ddd, J = 13.6, 4.3, 2.7 Hz, 1H), 1.83 (td, J = 13.7, 4.7 Hz, 1H), 1.71–1.54 (m, 5H), 1.54–1.44 (m, 3H), 1.44–1.38 (m, 2H), 1.36 (s, 3H), 1.33–1.29 (m, 2H), 1.28–1.18 (m, 2H), 1.15–1.13 (m, 6H), 1.12 (s, 3H), 1.00 (s, 3H), 0.80 (s, 6H), 0.74–0.66 (m, 1H). ^{13}C NMR (100 MHz, Chloroform-*d*): δ = 200.2, 176.9, 169.2, 128.6, 78.8, 61.8, 55.0, 51.8, 48.4, 45.4, 44.1, 43.2, 41.1, 39.2 (2C), 37.8, 37.1, 32.8, 31.9, 31.2, 28.5, 28.3, 28.1, 27.3, 26.5, 26.5, 23.4, 18.7, 17.5, 16.4, 15.6. $[\alpha]_D^{20}$ = +114.4233 ± 0.5225 in Chloroform. MS (ESI), *m/z* $[M + Na]^+$: 507.35. HRMS (ESI), *m/z* $[M + H]^+$: calculated for $C_{31}H_{49}O_4^+$485.3625; found 485.3611.

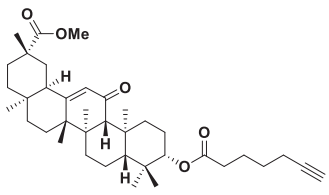

6-alkyne-heptyl-GAME (13): EDCI (42 mg, 0.22 mmol, 2.1 equiv), DMAP (7 mg, 0.05 mmol, 0.5 equiv), TEA (30 μL, 0.22 mmol, 2.1 equiv) and **GAME (12)** (50 mg, 0.11 mmol, 1.0 equiv) were added to a stirred solution of 6-heptynoic acid (21 μL, 0.17 mmol, 1.6 equiv) in dry DCM (1 mL). The mixture was stirred for at rt 24 h, then saturated NH_4Cl solution (10 mL) was added. The aqueous phase was extracted with DCM

(3 × 20 mL), then the collected organic phases were dried over Na_2SO_4 and concentrated under reduced pressure. Compound **13** was obtained with 49 % yield (29 mg) as a whitish solid after flash column chromatography purification (9:1*n*-hexane/ethyl acetate *v/v* as eluent). ^{1}H NMR (400 MHz, Chloroform-*d*): δ 5.66 (s, 1H), 4.52 (dd, J = 11.6, 4.8 Hz, 1H), 3.68 (s, 3H), 2.79 (dt, J = 13.6, 3.6 Hz, 1H), 2.38–2.29 (m, 3H), 2.21 (td, J = 7.0, 2.7 Hz, 2H), 2.11–2.04 (m, 1H), 2.01–1.88 (m, 3H), 1.88–1.54 (m, 12H), 1.49–1.38 (m, 3H), 1.36 (s, 3H), 1.32 (s, 1H), 1.29 (s, 1H), 1.25 (s, 1H), 1.16–1.13 (m, 6H), 1.12 (s, 3H), 1.07–0.97 (m, 2H), 0.89–0.86 (m, 6H), 0.80 (s, 3H). ^{13}C NMR (100 MHz, Chloroform-*d*): δ 182.4, 177.1, 173.3, 169.3, 128.7, 80.7, 68.7, 61.9, 55.2, 51.9, 48.6, 45.6, 44.2, 43.4, 42.7, 41.3, 38.9, 38.1, 37.9, 37.1, 34.4, 32.6, 31.9, 31.3, 29.9, 28.7, 28.5, 28.3, 28.0, 26.6, 24.3, 23.6, 23.4, 18.8, 18.3, 17.5, 16.9, 16.5. MS (ESI$^+$): *m/z* 615.40 [M + Na$^+$]. HRMS (ESI), *m/z* [M + H]$^+$: calculated for $C_{38}H_{57}O_5^+$593.4201; found 593.4223.

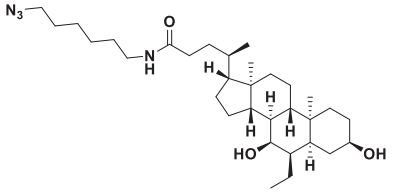

6-azidohexan-OCA (11): EDCI (45 mg, 0.23 mmol, 1.4 equiv), HOBt (31 mg, 0.23 mmol, 1.4 equiv), NMM (46 μL, 0.42 mmol, 2.5 equiv) and 6-azidohexan-1-amine (36 mg, 0.25 mmol, 1.5 equiv) were added to a stirred solution of obeticholic acid (70 mg, 0.17 mmol, 1.0 equiv) in dry DCM (1.6 mL). The mixture was stirred at rt for 24 h, then cooled down to 0 °C and 1 M HCl (10 mL) was added. The aqueous phase was extracted with EtOAc (3 × 20 mL), then the collected organic phases were and dried over Na_2SO_4 and concentrated under reduced pressure. Compound **11** was obtained with 60 % yield (54 mg) as a pale yellow solid after flash column chromatography purification (97:3 DCM/MeOH *v/v* as eluent). ^{1}H NMR (400 MHz, MeOD): δ 3.67 (s, 1H), 3.35–3.28 (m, 4H), 3.26–3.11 (m, 2H), 2.29–2.21 (m, 1H), 2.16–2.07 (m, 1H), 2.06–1.99 (m, 1H), 1.98–1.70 (m, 7H), 1.68–1.47 (m, 9H), 1.47–1.26 (m, 12H), 1.25–1.08 (m, 3H), 1.00 (d, J = 6.5 Hz, 3H), 0.96–0.88 (m, 6H), 0.71 (s, 3H). ^{13}C NMR (100 MHz, MeOD): δ 176.68, 73.19, 71.18, 57.40, 52.39, 51.68, 46.96, 43.76, 43.15, 41.55, 41.06, 40.21, 36.87, 36.79, 36.64, 34.53, 34.42, 34.18, 33.41, 31.26, 30.33, 29.85, 29.33, 27.53, 27.51, 24.58, 23.77, 23.49, 21.98, 18.92, 12.30, 12.04. $[\alpha]_D^{20}$ = +6.5577 ± 0.6030 in Chloroform. MS (ESI$^+$): *m/z* 567.42 [M + Na$^+$]. HRMS (ESI), *m/z* [M + H]$^+$: calculated for $C_{32}H_{57}N_4O_3^+$545.4425; found 545.4439.

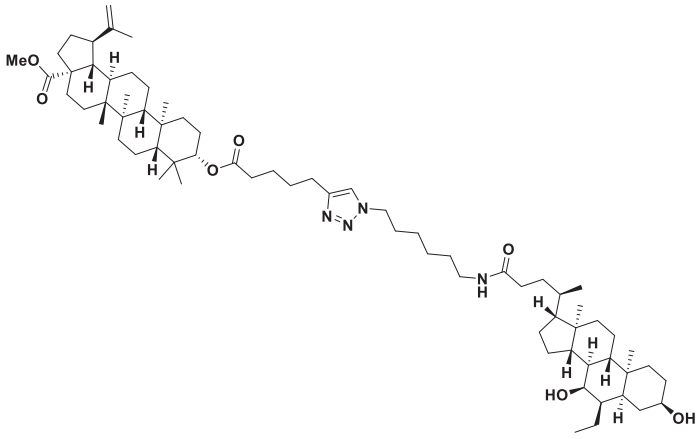

Triazole-BAME-OCA (3): **11** (42 mg, 0.08 mmol, 1.0 equiv), **10** (65 mg, 0.11 mmol, 1.35 equiv), $CuSO_4{\cdot}5H_2O$ (4 mg, 0.016 mmol, 0.2 equiv) and sodium ascorbate (17 mg, 0.08 mmol, 1.0 equiv) were dissolved in THF/H_2O 1:1 (1.2 mL, *v/v*). The mixture was stirred at rt for 24 h, then concentrated under reduced pressure. Compound **3** was obtained with 61 % yield (55 mg) as a white solid after flash column chromatography purification (97:3 DCM/MeOH *v/v* as eluent). ^{1}H NMR (400 MHz, MeOD): δ 7.76 (s, 1H), 4.75 (d, J = 2.3 Hz, 1H), 4.66–4.62 (m, 1H), 4.48 (dd, J = 10.6, 5.7 Hz, 1H), 4.39 (t, J = 7.0 Hz, 2H), 3.69 (s, 4H), 3.21–3.14 (m, 2H), 3.03 (td, J = 10.8, 4.6 Hz, 1H), 2.75 (t, J = 6.9 Hz, 2H), 2.38 (t, J = 6.8 Hz, 2H), 2.32–2.21 (m, 2H), 2.17–2.08 (m, 1H), 2.07–2.00 (m, 1H), 1.97–1.82 (m, 10*H*), 1.81–1.61 (m, 17H), 1.60–1.26 (m, 36H), 1.05 (s, 3H), 1.01 (d, J = 6.5 Hz, 3H), 0.98 (s, 3H), 0.96 (s, 4H), 0.94 (s, 2H), 0.93 (s, 3H), 0.90–0.85 (m, 6H), 0.72 (s, 3H). ^{13}C NMR (100 MHz, MeOD): δ 178.0, 176.6, 175.0, 151.7, 123.1, 110.4, 82.3, 73.2, 71.2, 57.9, 57.4, 56.8, 51.8, 51.7, 51.1, 50.6, 49.0, 48.5, 46.9, 43.8, 43.6, 43.2, 41.9, 41.6, 41.1, 40.1, 39.6, 39.6, 38.9, 38.3, 37.9, 36.9, 36.8, 36.7, 35.5, 35.2, 34.5, 34.4, 34.2, 33.4, 33.2, 31.7, 31.3, 31.2, 30.8, 30.2, 29.9, 29.4, 28.6, 27.3, 27.1, 26.8, 25.9, 25.6, 24.8, 24.6, 23.9, 23.5, 22.1, 22.0, 19.7, 19.3, 19.0, 17.1, 16.8, 16.6, 15.3, 12.4, 12.1. $[\alpha]_D^{20}$ = +10.6280 ± 1.2519 in Chloroform. MS (ESI$^+$): *m/z* 1123.98 [M + H$^+$]. HRMS (ESI), *m/z* [M + H]$^+$: calculated for $C_{70}H_{115}N_4O_7^+$1123.8760; found 1123.8744.

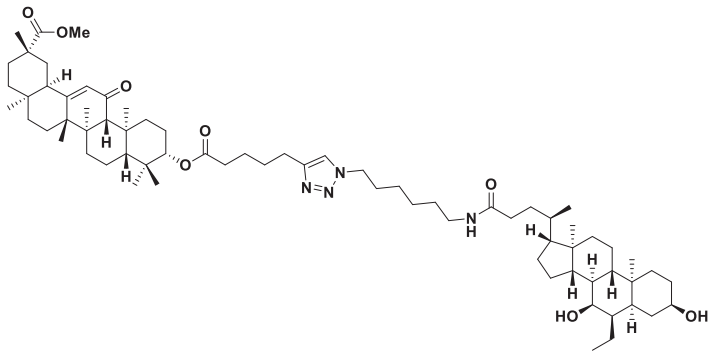

Triazole-GAME-OCA (4): **11** (25 mg, 0.05 mmol, 1.0 equiv), **13** (30 mg, 0.05 mmol, 1.0 equiv), $CuSO_4{\cdot}5H_2O$ (4 mg, 0.01 mmol, 0.2 equiv) and sodium ascorbate (10 mg, 0.05 mmol, 1.0 equiv) were dissolved in THF/H_2O 1:1 (1.0 mL, *v/v*). The mixture was stirred at rt for 24 h, then concentrated under reduced pressure. Compound **4** was obtained with 56 % yield (32 mg) as a white solid after flash column chromatography purification (98:2 DCM/MeOH *v/v* as eluent). ^{1}H NMR (400 MHz, Chloroform-*d*): δ 7.31 (s, 1H), 5.66 (s, 1H), 5.58 (s, 1H), 4.51 (dd, J = 11.6, 4.8 Hz, 1H), 4.32 (t, J = 6.8 Hz, 2H), 3.69 (s, 4H), 3.40 (tt, J = 10.4, 4.9 Hz, 1H), 3.22 (q, J = 6.6 Hz, 2H), 2.84–2.72 (m, 3H), 2.40–2.31 (m, 3H), 2.28–2.17 (m, 2H), 2.13–1.54 (m, 40H), 1.51–1.38 (m, 14H), 1.36 (s, 3H), 1.25 (s, 6H), 1.18–1.14 (m, 6H), 1.12 (s, 3H), 1.06–0.98 (m, 4H), 0.94–0.91 (m, 3H), 0.90–0.88 (m, 3H), 0.87–0.86 (m, 3H), 0.80 (s, 3H), 0.65 (s, 3H). ^{13}C NMR (100 MHz, Chloroform-*d*): δ 202.2, 177.4, 174.4, 173.5, 169.6, 147.8, 128.5, 121.9, 80.5, 72.3, 70.8, 61.7, 55.8, 55.0, 51.8, 50.5, 48.4, 45.4, 45.2, 44.1, 43.2, 42.7, 41.2, 41.1, 40.1, 39.8, 39.1, 38.8, 38.1, 37.7, 36.9, 35.5, 34.4, 34.0, 33.6, 33.3, 32.7, 31.8, 31.1, 30.6, 30.1, 29.7, 29.4, 28.8, 28.5, 28.3, 28.3, 28.1, 26.5, 26.4, 26.1, 26.0, 25.5, 25.3, 24.6, 23.7, 23.6, 23.4, 23.2, 22.3, 21.1, 20.8, 18.8, 18.7, 18.4, 17.4, 16.8, 16.4, 11.8, 11.7. $[\alpha]_D^{20}$ = +59.7687 ± 2.7960 in Chloroform. MS (ESI$^+$): *m/z* 1138.56 [M + H$^+$]. HRMS (ESI), *m/z* [M + H]$^+$: calculated for $C_{70}H_{113}N_4O_8^+$1137.8553; found 1137.8541.

CRediT authorship contribution statement

Martina Pedrini: Investigation, Data curation. **Luca Pozzi:** Writing – review & editing, Writing – original draft, Methodology, Data curation. **Francesca Sacchi:** Investigation, Data curation. **Andrea Citarella:** Writing – review & editing, Writing – original draft, Visualization, Project administration, Methodology, Investigation, Formal analysis, Data curation, Conceptualization. **Valerio Fasano:** Supervision. **Pierfausto Seneci:** Supervision. **Stefano Pieraccini:** Writing – original draft, Supervision. **Lorenzo Ruberto:** Writing – original draft, Visualization, Software, Methodology, Investigation, Formal analysis. **Helena Perez Peña:** Software, Methodology, Investigation, Formal analysis. **Alfredo Garzino-Demo:** Writing – review & editing, Funding acquisition. **Adriana Vitiello:** Writing – review & editing, Investigation, Data curation. **Leonardo Sernicola:** Investigation. **Alessandra Borsetti:** Writing – review & editing, Formal analysis. **Arianna Calistri:** Writing – review & editing, Formal analysis. **Cristina Parolin:** Writing – review & editing, Resources, Funding acquisition, Formal analysis. **Daniele Passarella:** Writing – review & editing, Supervision, Resources, Project administration, Investigation, Funding acquisition.

Funding

This study was supported by PARO_FINA20_01 to C.P., the Italian Ministry of University, project of relevant national interest (PRIN): 2020LW7X to A.G.-D.

Declaration of competing interest

The authors declare that they have no known competing financial interests or personal relationships that could have appeared to influence the work reported in this paper.

Acknowledgement

We thank Maria Vittoria Fornaini, Department of Molecular Medicine, University of Padova, for graphical help with Fig. 5.

Appendix A. Supplementary material

Supplementary data to this article can be found online at https://doi.org/10.1016/j.bmc.2025.118124.

Data availability

Data will be made available on request.

References

1. Lefkowitz EJ, et al. Virus taxonomy: the database of the International Committee on Taxonomy of Viruses (ICTV). *Nucleic Acids Res.* 2018;46:D708–D717.
2. Maier HJ, Bickerton E, Britton P. Coronaviruses: methods and protocols; 2015.
3. MacLachlan NJ, Dubovi E. CORONAVIRUSES of birds. Fenner's Vet. *Virology.* 2017: 435–461.
4. Zhu N, et al. A novel coronavirus from patients with pneumonia in China, 2019. *N Engl J Med.* 2020;382:727–733.
5. COVID-19 Map - Johns Hopkins Coronavirus Resource Center, https://coronavirus.jhu.edu/map.html.
6. Jackson CB, Farzan M, Chen B, Choe H. Mechanisms of SARS-CoV-2 entry into cells. *Nat Rev Mol Cell Biol.* 2022;23:3–20.
7. Walls AC, et al. Structure, function, and antigenicity of the SARS-CoV-2 spike glycoprotein. *Cell.* 2020;181:281–292.e6.
8. Wrapp D, et al. Cryo-EM structure of the 2019-nCoV spike in the prefusion conformation. *Science.* 2020;367:1260–1263.
9. Li F. Structure, function, and evolution of coronavirus spike proteins. *Annu Rev Virol.* 2016;3:237–261.
10. Huang Y, Yang C, Xu X, Xu W, Liu SW. Structural and functional properties of SARS-CoV-2 spike protein: potential antivirus drug development for COVID-19. *Acta Pharmacol Sin.* 2020;41:1141–1149.
11. Hoffmann M, et al. SARS-CoV-2 cell entry depends on ACE2 and TMPRSS2 and is blocked by a clinically proven protease inhibitor. *Cell.* 2020;181:271–280.
12. Lan J, et al. Structure of the SARS-CoV-2 spike receptor-binding domain bound to the ACE2 receptor. *Nature.* 2020;581:215–220.
13. Carino A, et al. Hijacking SARS-CoV-2/ACE2 receptor interaction by natural and semi-synthetic steroidal agents acting on functional pockets on the receptor binding domain. *Front Chem.* 2020;8:1–15.
14. Citarella A, et al. Synthesis of SARS-CoV-2 Mpro inhibitors bearing a cinnamic ester warhead with in vitro activity against human coronaviruses. *Org Biomol Chem.* 2023; 21:3811–3824.
15. Citarella A, et al. Discovery of a novel trifluoromethyl diazirine inhibitor of SARS-CoV-2 Mpro. *Molecules.* 2023;28:1–8.
16. Citarella A, et al. Pseudo-dipeptide bearing α,α-difluoromethyl ketone moiety as electrophilic warhead with activity against coronaviruses. *Int J Mol Sci.* 2021;22: 1–17.

17. Citarella A, et al. Synthesis of α-fluorocinnamate derivatives as novel cathepsin S inhibitors with in vitro antiproliferative activity against pancreatic cancer cells. *Bioorg Med Chem*. 2024;115, 117987.
18. Boiarska Z, et al. Maytansinol functionalization: towards useful probes for studying microtubule dynamics. *Chem A Eur J*. 2023;29.
19. Amenta A, et al. Recent advances in the development of CB1R selective probes. *Front Nat Prod*. 2023;2:1–14.
20. Ozono S, et al. SARS-CoV-2 D614G spike mutation increases entry efficiency with enhanced ACE2-binding affinity. *Nat Commun*. 2021;12, 848.
21. Viana R, et al. Rapid epidemic expansion of the SARS-CoV-2 Omicron variant in southern Africa. *Nature*. 2022;603:679–686.
22. Sarkar M, Madabhavi I. COVID-19 mutations: an overview. *World J Methodol*. 2024; 14:1–17.
23. Bonandi E, et al. The 1,2,3-triazole ring as a bioisostere in medicinal chemistry. *Drug Discov Today*. 2017;22:1572–1581.
24. Crawford KHD, et al. Protocol and reagents for pseudotyping lentiviral particles with SARS-CoV-2 spike protein for neutralization assays. *Viruses*. 2020;12:1–15.
25. Liu Y, et al. An infectivity-enhancing site on the SARS-CoV-2 spike protein targeted by antibodies. *Cell*. 2021;184:3452–3466.
26. Abagyan R, Kuznetsov D, Totrov M. ICM - new method for protein modeling and design: applications to docking and structure prediction from the distorted native conformation. *J Comput Chem*. 1994;15:488–506.
27. Abagyan R, Totrov M. Biased probability Monte Carlo conformational searches and electrostatic calculations for peptides and proteins. *J Mol Biol*. 1994;235:983–1002.
28. Totrov M, Abagyan R. Derivation of sensitive discrimination potential for virtual ligand screening. In: *ACM Press the third annual international conference - Lyon, France*. 1999:312–320.